Modeling and inversion with semi-airborne electromagnetic method for imaging subsurface structures

Bayat, M.[1], Ronczka, M.[1], Nazari, S.[1], Rochlitz, R.[1], Guenther, T. [1]
[1] LIAG-Institute for Applied Geophysics, Hannover, Germany, contact: Maryam.Bayat@leibniz-liag.de

SUMMARY

Electromagnetic surveys can be employed in different ways such as ground-based, airborne, or semi-airborne, each offering unique capabilities for imaging the subsurface. Semi-airborne electromagnetic (sAEM) methods provide a balance between resolution and depth penetration compared to the other two options. They have the advantage of avoiding difficult terrains or rough topographies, such as mountainous regions, forests, and rivers in comparison with ground-based surveys. Another advantage of sAEM is a larger investigation depth due to a stronger source signal and a larger Tx-Rx distance, however, it is limited in terms of covered survey area compared to airborne methods. For creating nuclear waste disposals, subsurface structures like clay layers act as impermeable barriers, affecting fluid flow dynamics and trapping subsurface fluid. Detecting these structures aids in predicting fluid migration and assessing environmental risks. We have studied the electromagnetic response of conductive clay layers and a fault zone by simulating both helicopter and drone surveys with the sAEM method. This study aims to enhance our understanding of the subsurface geology by characterizing a fault structure and delineating clay layers using sAEM. We used the modeling tool custEM to generate synthetic data. After validation of forward models through semi-analytical solutions, inverse models were calculated. The findings indicate that this technique is effective in capturing high-resolution details of near-surface features and investigating deeper subsurface layers.

Keywords: Semi-airborne electromagnetics, forward modeling, inverse modeling, geophysical modeling

INTRODUCTION

Electromagnetic (EM) methods in geophysics utilize the principles of electromagnetism to provide insights into subsurface properties through electrical resistivity. These methods are used in geological mapping, geotechnical investigations, environmental and groundwater studies. Since the last decades, marine, ground-based, and airborne controlled-source electromagnetics (CSEM) have been employed from simple soundings to complicated setups with multiple sources and receivers for large-scale multidimensional investigations. The sAEM as an EM survey method has recently been used in geological mapping as it integrates the advantages of airborne receivers (Rx) along with strong ground-based transmitters (Tx). The frequency of the signal, Tx-Rx offset, and subsurface electrical resistivity distribution affect the depth of penetration. Compared to airborne systems, sAEM has more penetration depth since it uses ground-based Tx which sends high signal amplitudes at low frequencies even if the Tx-Rx offset is large (Smith et al. 2001).

In this study, the sAEM method was utilized to model impermeable layers and a fault zone, which affect fluid flow dynamics and trapping subsurface fluid, in different scales with the aim of predicting fluid migration and assessing environmental risks. The synthetic modeling framework enables the creation of detailed subsurface conductivity models, which can be used to analyze the electromagnetic responses.
Simulations are performed with the open-source python toolbox, custEM, to solve the total-field formulation of the Maxwell equations based on an accurate second-order finite-element (FE) forward operator (Rochlitz et al. 2019). To simulate real-world conditions, random noise of 5% plus 2 pT/A absolute noise were added to the synthetic data. Inversion results have been created with the inversion approach based on custEM and pyGIMLi (Rochlitz et al. 2023).

METHODOLOGY

CSEM methods use frequencies less than 10 kHz, therefore, the quasi-static approximation of Maxwell's equations is valid. Combining Ampere's and Faraday's law yields the Helmholtz equation in terms of the electric field.

$$\nabla\times\mu^{-1}\nabla\times\mathbf{E} + i\omega\sigma\mathbf{E} = -i\omega\mathbf{J}_e \quad (1)$$

Where $\mathbf{E}$ denotes the total electric field, ω is the angular frequency, σ is the electric conductivity, μ is the magnetic permeability, and $\mathbf{J}_e$ is the source current density.
The Helmholtz equation in terms of magnetic field $\mathbf{H}$ is as Equation (2).

$$\nabla\times\sigma^{-1}\nabla\times\mathbf{H} + i\omega\mu\mathbf{H} = \nabla\times\sigma^{-1}\mathbf{J}_e \quad (2)$$

In sAEM, depicted in Figure 1, a powerful transmitter located on the ground generates primary electromagnetic fields that penetrate into the earth. An airborne receiver, typically mounted on a helicopter or drone, flies over the survey area to detect the secondary electromagnetic fields induced in the subsurface by these primary fields. The primary data collected are electromagnetic field responses at various frequencies, which are then analyzed in the frequency domain. The frequency-domain data are processed and inverted to create subsurface resistivity models, revealing geological structures and variations.

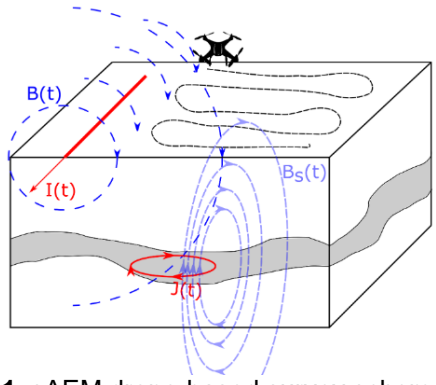

Figure 1. sAEM drone-based survey scheme.

MODELS AND RESULTS

Two different models, a clay layer and a fault zone, in helicopter and drone scales were synthetically created to study the capability of sAEM method in detecting geological and environmental settings.

Model 1: Clay layer

- intact layer
- same layer with a hole inside

Both clay layers were modelled based on a helicopter survey. Two parallel ground-based transmitters with a length of 3.4 km along y direction were used. The total 421 receiver points cover an area of 9 km^2 (21 points in ea line in both x and y direction). The distance between flight lines was considered 150 m and the helicopter height was 80 m. The dimension of the clay layer was 7000m×7000m×200m while its depth was set to 600 m. In both models the electrical resistivity of the background was set to 100 Ωm and the anomaly, clay layer, to 5 Ωm.
For the second case we used the same dimensions as before and only added a hole with the size of 1600m x 1600m with a center at (0, 0, 0). To make the comparison possible, for the clay layer with a hole inside all parameters were set similar to the clay layer to see how the hole affects the magnetic field response. A frequency range from 8 to 1024 Hz was used for modeling. We set receiver lines at a distance of 400 m from transmitters to reduce artifacts due to the effects of the primary fields near transmitters (Nazari et al. 2023).

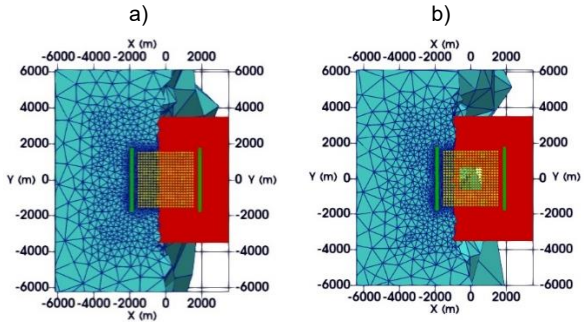

Figure 2. Meshes and location of the layers (red), receivers (yellow points), and transmitters (green lines) for a) clay layer, b) clay layer with a hole.

Figure 3 depicts x and z components of the magnetic field for models in the Figure 2. 1D models are the responses of the homogeneous half space, which are semi analytical responses, and considered as validations of the simulated 3D models. The misfit term in Figure 1.e is the computational noise, while in the Figure 1.f it is the effect of the hole in the imaginary part of the Bx misfit term. The larger the size of the hole, the greater its impact on the misfit. Typically, the misfit tends to be lower for larger transmitter offsets due to the assigned relatively higher error floor.

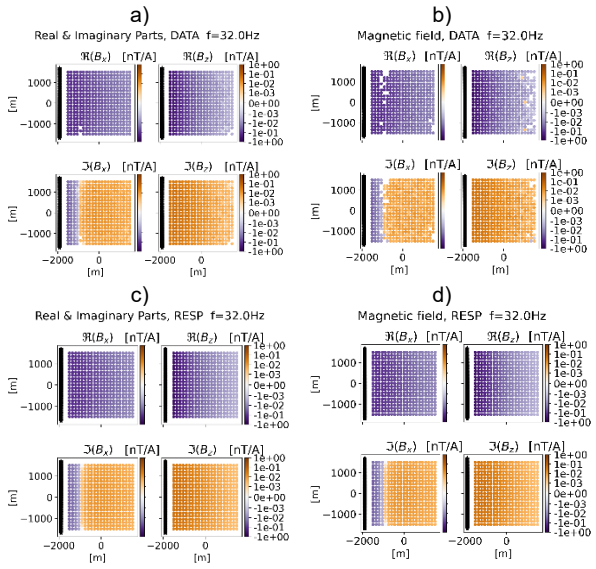

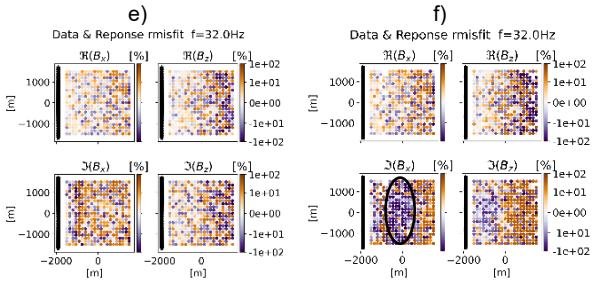

Figure 3. Forward response of clay layers at 32 Hz using only the left transmitter. a and b) the forward response of the real and imaginary parts of the Bx and Bz fields for the synthetic data (3D responses), c and d) the semi-analytical (1D) responses, which are identical for both models. e and f) the misfit terms between the data and responses for the intact layer and the layer with a hole, respectively.

As a measure of how well the data fits, we used the Chi-square (χ^2) value, which ideally should be around 1 for synthetic modeling. The regularization parameter, λ, which balances the trade-off between data fit and model smoothness, was set to 1 with a factor of 0.8 for each iteration. The χ^2 values ended at 1.14 and 1.34 with computation times of approximately 4.5 and 4.5 hours for the intact clay layer and the clay layer with a hole, respectively.

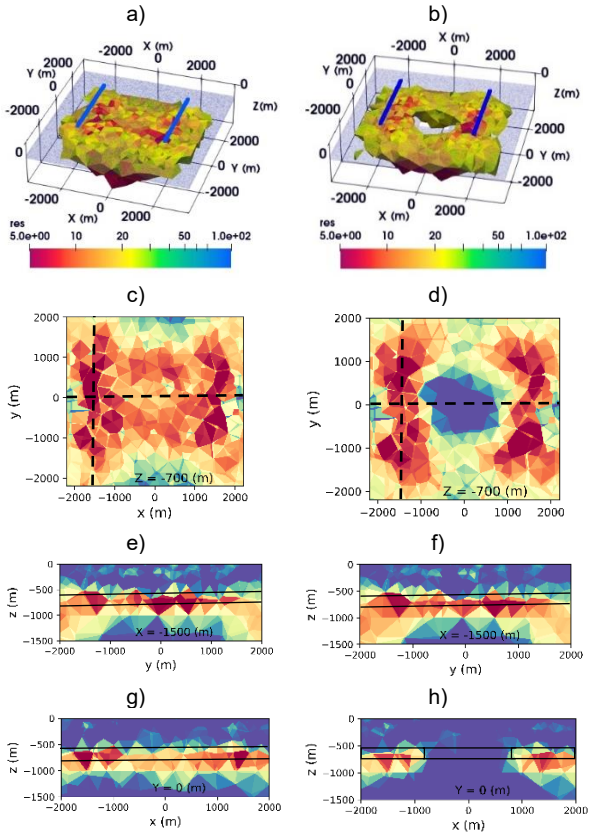

Figure 4. Inversion results for the specified layers using both transmitters. a and b) good conductors (<25 Ωm). Thick blue lines are transmitter lines. c and d) slices at Z = -700 m. Dashed lines show where the x and y slices are extracted. e and f) slices at X = -1500 m, and g and h) slices at Y = 0.

Model 2: Fault zone

The fault zone was modeled using synthetic data from a drone-based survey. Two parallel ground-based transmitters, each 1 km long, along y direction were employed. A total number of 625 receiver points covered an area of 1.44 km², with 25 points along each line in both x and y directions and 50 m line spacing. The height of drone was considered 30 m. The faulted layer, representing the anomaly, was 2000×1600×100 m³ with a depth of 100 m for the up-lifted layer and 180 m for the down-lifted layer. The modeling utilized frequencies range from 100 Hz to 10 kHz. The electrical resistivity of the background and faulted layer were assumed 400 and 5 Ωm, respectively. In comparison to a helicopter-based modeling, the minimum distance of 200 m between receiver lines and transmitters is shorter.

Figure 5 illustrates the results for two different frequencies to assess the impact of frequency on the data. For both responses only the left side transmitter was considered. Higher frequencies result in increased noise, which leads to data loss. Consequently, the data quality deteriorates at higher frequencies.

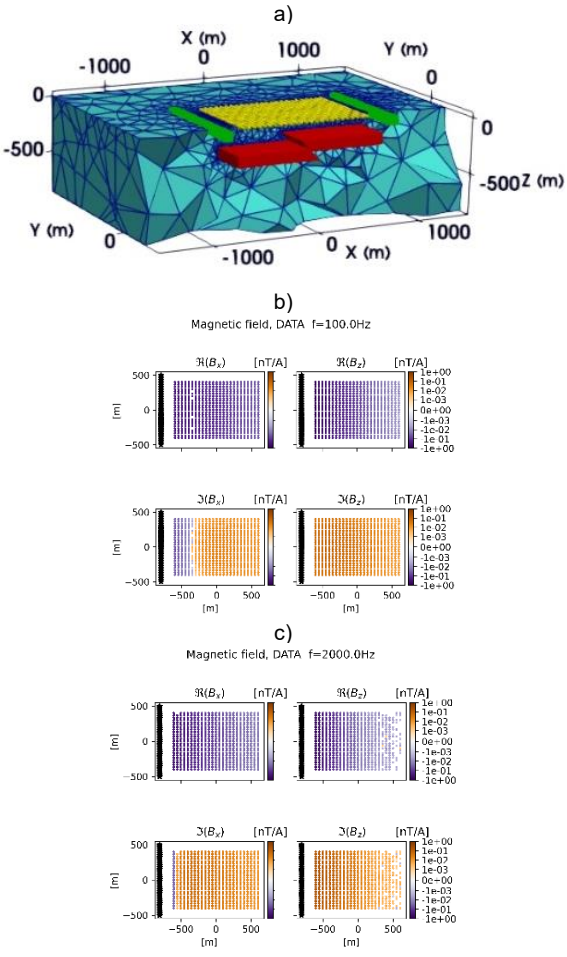

Figure 5. a) Meshes and locations of the faulted layer (shown in red), receivers (yellow points), and transmitters (green lines). Forward response of the fault zone was shown at b) 100 Hz, c) and 2 kHz.

The 3D inversion result of the fault zone is shown in Figure 6, where the Y slice at -60 m (Figure 6.d) clearly shows the disruption and transformation of a straight layer into a fault zone. The final χ^2 value was 1.30 with the execution time of approximately 4 hours.

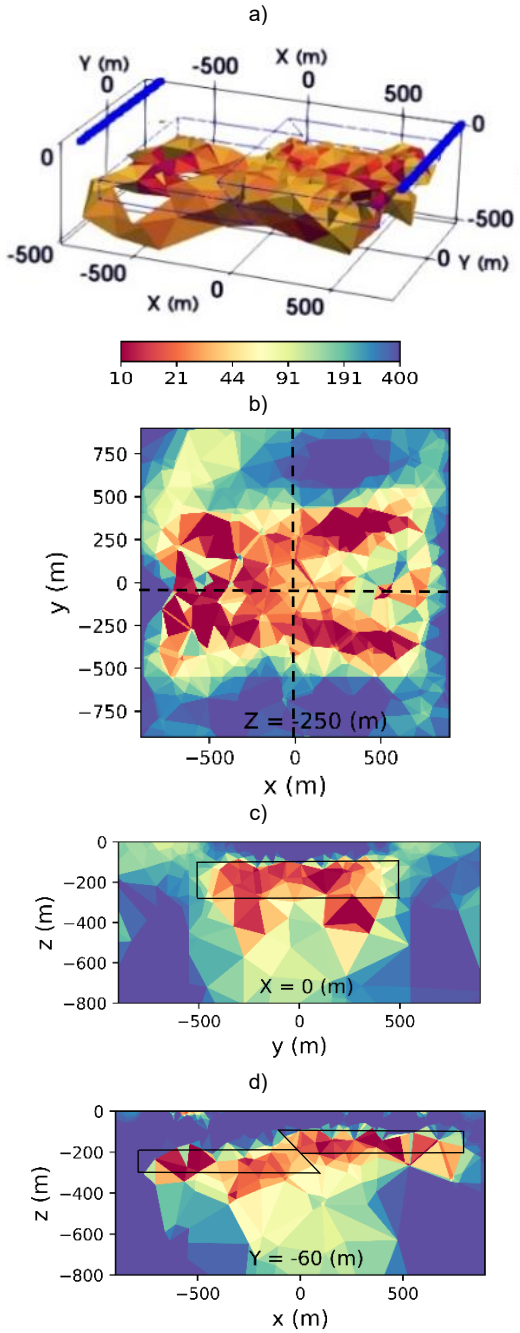

Figure 6. 3D Inversion result for the faulted layer using both transmitters. a) The good conductor (<30 Ωm). Thick blue lines are transmitters and thin lines are the outline of the faulted layer, b) slice at Z = -150 m, c) slice at X = 0, d) slice at Y = -60 m.

CONCLUSIONS

We created synthetic models including clay layers and a fault zone indifferent scales to study the capability of the sAEM method in imaging subsurface structures, paving the way for improved understanding of geological processes and environmental challenges with high resolution and delving into deeper subsurface layers. It is important to acknowledge that while these findings are reliable for synthetic models, real-world data complexities may yield different and more complicated results.

ACKNOWLEDGEMENTS

The project GeoMetEr is funded by the Federal Company for radioactive waste disposal (BGE).

REFERENCES

Nazari S, Rochlitz R, Günther T (2023) Optimizing Semi-Airborne Electromagnetic Survey Design for Mineral Exploration. Minerals, 13, 796.

Rochlitz R, Skibbe N, Günther T (2019) custEM: Customizable finite-element simulation of complex controlled-source electromagnetic data. Geophysics, 84, F17–F33.

Rochlitz R, Becken M, Günther T (2023) Three-dimensional inversion of semi-airborne electromagnetic data with a second-order finite-element forward solver. Geophysical Journal International 234 (1), 528-545.

Smith R.S, Annan A.P. & McGowan, P.D (2001) A comparison of data from airborne, semi-airborne and ground electromagnetic systems. Geophysics, 66(5), 1379–1385.